Mobility analysis of structure-borne noise power flow through bearings in gearbox-like structures

Todd E. Rook and Rajendra Singh[a)]

(Received 1995 April 19; revised 1995 December 04; accepted 1996 February 14)

A narrow-band vibratory power flow calculation procedure based on the mobility method is described which recognizes rolling element bearings as a multi-dimensional compliant and dissipative connection. A gearbox with rigid casing, compliant mounts, one spur gear pair, and four bearings is analyzed and concepts for reduced noise and vibration are identified. Some pertinent modeling issues that are related to the truncated modal bases of components being synthesized are discussed. An experimental system which conceptually simulates the structure-borne noise phenomena of a gearbox is also studied. The proposed theory has been found to agree well with limited measurements. ***© 1996 Institute of Noise Control Engineering.***

Primary subject classification: 43.2.1; Secondary subject classification: 76.9

1. INTRODUCTION

The role of bearings as transmitters of structure-borne noise in rotating machinery or equipment is not well understood. This shortcoming must be overcome before quiet products may be designed, and is of particular importance for mechanical drives in automotive, aerospace, or industrial applications where structural paths are especially dominated. For instance, Brandl *et al.* emphasized the importance of bearings while discussing strategies for low noise engines.[1] Several authors[2–5] have reported a range of radiated sound levels in geared systems with alternate rolling element bearings. However, empirical studies have led to ambiguities in the choice of bearings. Historically, bearings have been selected in industry from a reliability and tribological viewpoint, and even today very little consideration is given to their dynamical or acoustical behavior. Consequently, a designer has few analytical tools with which to rate the *in-situ* noise performance of rolling element bearings in mechanical equipment. The situation is further confused by conflicting empirical design rules that are widely used.[6]

Typically, bearings have been modeled as ideal boundary conditions or scalar springs and dampers, even though such models significantly underestimate their complexity. Lim and Singh proposed a new stiffness matrix of dimension 6 which describes the motion or force transmissibility across rolling element bearings.[7] The theory was embedded in a model based on statistical energy analysis with many simplifying assumptions. This broadband approach, though partially successful in predicting the coupling loss factors, does not yield sufficient mechanical system design information to address complex machinery noise problems at lower frequencies. As a consequence, a narrow-band approach that retains spatial and spectral resolution is needed. The purpose of this paper is to incorporate the bearing stiffness matrix formulation into an overall calculation procedure to describe the related structure-borne noise power flow problem in the context of a mechanical system such as a gearbox. On a more fundamental note, it is recognized that rolling element bearings belong to a family of multi-dimensional, non-ideal compliant and dissipative connections. A new methodology, based on a structural mobility approach, will be developed to facilitate the evaluation of a particular bearing design from the noise and vibration control viewpoint. A simplified gearbox-like structure is analytically and experimentally studied as a first step toward the overall solution.

2. PROBLEM FORMULATION

In order to illustrate the structure-borne noise power flow calculations, two example cases will be discussed. The first model describes a gearbox with rigid casing, compliant mounts, and four bearing connections and is shown in Fig. 1. The second model shown in Fig. 2, is intended for experimental studies. It is a phenomenological structural model of the gearbox that includes multiple moment and force path transmissions. The scope of the acoustical analysis is restricted to low and medium frequencies on a narrow-band basis since modulated pure tones, which also excite system resonances, are often radiated by gearboxes.

To investigate the power flow through bearings and non-ideal joints, there are several requirements which any po-

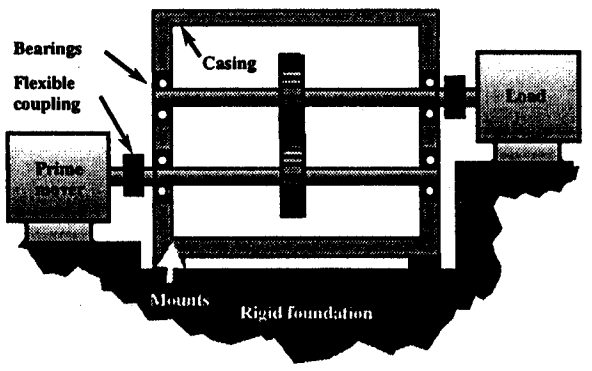

Fig. 1 – Schematic of a simplified gearbox.

[a)] *Acoustics & Dynamics Laboratory, Department of Mechanical Engineering, The Ohio State University, Columbus, Ohio 43210-1107, U.S.A.*

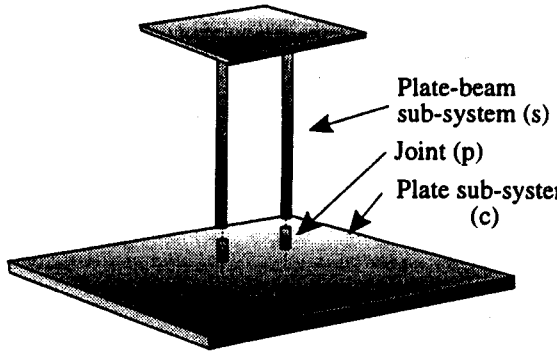

Fig. 2 – Experimental setup. See Fig. 3 for the identification of (s), (p), and (c).

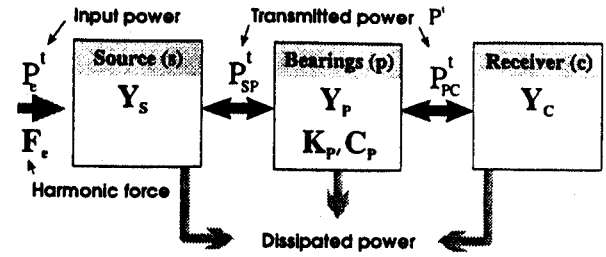

Fig. 3 – Schematic of source–path–receiver model. All connections are multi-dimensional.

tential method of analysis must satisfy. A component synthesis technique is obviously desirable in order to facilitate quick interchangability of the bearings. Additionally, since bearings and joints transmit moments as well as forces, vector rather than scalar type paths must be described. Furthermore, a method which permits different damping values among components is needed. For narrow-band power flow calculations, either a mobility approach[8–10] or the modal synthesis technique[11] must be employed. A detailed review of several such approaches can be found in a recent article.[11] Several existing techniques are basically modal analysis techniques that are also used to calculate the power flow between substructures; however modal analysis itself is not crucial to the power flow calculations. Unfortunately, most of these techniques also tend to obscure design changes in individual components and do not satisfy many of the aforementioned requirements in their present form. Therefore, refinements to the mobility method which overcome such deficiencies are proposed. The refinements are based on the full mobility matrices **Y** at the connection points between components or substructures. Thus, they account for transfer mobilities which previous studies ignored.[10] Moreover, unlike prior work,[8–12] the refined method includes non-ideal joints by defining vector paths. Since the number of degrees of freedom at the connection points is much less than the total number of degrees of freedom of the structure, this method is more tractable than prior approaches.[11,12] With the current method, eigenanalyses are only performed on the components; no further eigenanalysis of the assembled components is necessary as was the case in previous methods.[11,12] In the spirit of developing a computationally efficient scheme, Guyan reduction was used on each of the substructures in the calculation of the mobilities. Other than this dynamic reduction, the synthesis procedure is exact. Recent articles[13,14] by the authors describe the methodology in detail. Here, only application specific mathematical models are presented along with a condensed version of the techniques for the sake of completeness.

3. POWER FLOW THROUGH BEARINGS

Figure 3 can be used to conceptually describe the power flow for the systems of Figs. 1 and 2. In the case of Fig. 1, the rotating system (including the gears, shafts, prime mover, and load) is considered to be the source while the casing is considered to be the receiving structure which interacts with flexible mounts or the foundation. The mobility approach is not concerned with the internal behavior of the particular components. Instead, the mobility approach only requires the interfacial structural mobilities **Y**, forces **F**, and velocities **v**. Here bold symbols denote matrices or vectors of dimension n. Free–free boundary conditions on each component are assumed in the calculation of the mobility matrices. To simplify the problem, many prior investigators[10] have neglected the transfer mobilities when studying multiple connections with mobility approaches. Such an approximation serves to uncouple the joint locations so that only driving-point mobilities are used. However this approximation is not applicable at the lower frequencies which are of particular interest here. As a result, the full component mobility matrices including transfer mobilities are retained in this study.

The mobility procedure will be developed as follows. For narrow-band analysis, first the following equations are defined in the frequency domain (ω), with reference to Fig. 3:

$$\begin{Bmatrix} \mathbf{v}_e(\omega) \\ \mathbf{v}_{sp}(\omega) \end{Bmatrix} = \begin{bmatrix} \mathbf{Y}_S^{11}(\omega) & \mathbf{Y}_S^{12}(\omega) \\ \mathbf{Y}_S^{21}(\omega) & \mathbf{Y}_S^{22}(\omega) \end{bmatrix} \begin{Bmatrix} \mathbf{F}_e(\omega) \\ -\mathbf{F}_{sp}(\omega) \end{Bmatrix}, \tag{1a}$$

$$\mathbf{v}_{pc}(\omega) = \mathbf{Y}_c(\omega)\mathbf{F}_{pc}(\omega), \tag{1b}$$

$$\begin{Bmatrix} \mathbf{v}_{sp}(\omega) \\ \mathbf{F}_{sp}(\omega) \end{Bmatrix} = \begin{bmatrix} \mathbf{I} & \mathbf{Y}_p(\omega) \\ \mathbf{0} & \mathbf{I} \end{bmatrix} \begin{Bmatrix} \mathbf{v}_{pc}(\omega) \\ \mathbf{F}_{pc}(\omega) \end{Bmatrix}, \tag{1c}$$

where **I** is the identity matrix and the superscripts 11, 12, 21, and 22 denote the submatrices for the input (1) and output (2) ports/interfaces of a component. Furthermore, $\mathbf{v}_e$ is the velocity vector of dimension n_e at the excitation (e) interface, $\mathbf{v}_{sp}$ is the velocity vector of dimension n_p at the source(s)-bearing path(p) interface, and $\mathbf{v}_{pc}$ is the velocity vector of dimension n_p of the bearing path(p)–free receiver(c) interface. The interfacial force vectors are defined analogously. It should be pointed out that the method is generic enough to accept n_e uncorrelated excitations (e.g. internal displacement excitation or external torque), but only sinusoidal displacement excitation of amplitude ε will be considered in this study for the sake of brevity. In this case $\mathbf{F}_e(\omega) = \omega^2\varepsilon$. Consequently, $\mathbf{Y}_s$ is of dimension $n_e + n_p$, $\mathbf{Y}_c$ is of dimension n_p, and $\mathbf{Y}_p$ is of dimension n_p.

The bearing paths are considered massless, and are characterized by their stiffness, $\mathbf{K_p}$, and damping, $\mathbf{C_p}$, matrices, which are of dimension n_p and are assumed symmetric for the sake of convenience. The modeling of the bearings as massless and spatially discrete is valid for lower frequencies, and is consistent with the specification of a narrowband approach such as the mobility/receptance methods.[8-10] Note that to avoid using a singular mobility matrix of dimension $2n_p$ in Eq. (1c), the bearings' equations are posed in the form of a transfer matrix with a non-singular $\mathbf{Y_p}=i\omega(\mathbf{K_p}+i\omega\mathbf{C_p})^{-1}$ of dimension n_p. Couplings between degrees of freedom are permitted for these general connections and each bearing may be represented by a 6×6 matrix, which may then be reduced further in dimension depending on symmetry.

Assembling the mobility matrices of Eq. (1) and solving for the interfacial forces yields

$$\begin{Bmatrix}\mathbf{F_e}(\omega)\\ \mathbf{F_p}(\omega)\end{Bmatrix}=\begin{bmatrix}\mathbf{I}\\ \mathbf{\Gamma}(\omega)\end{bmatrix}\mathbf{F_e}(\omega), \tag{2}$$

where the intermediate matrices

$$\mathbf{\Gamma}(\omega)=(\mathbf{Y_s^{22}}(\omega)+\mathbf{Y_p}(\omega)+\mathbf{Y_c}(\omega))^{-1}\mathbf{Y_s^{21}}(\omega) \tag{3}$$

result from the inversion of mobility matrices in terms of the submatrices.[13] This economizes the method since all operations are then performed on the smaller component matrices. Furthermore, the interfacial velocities may be obtained from these interfacial forces through the equation

$$\begin{Bmatrix}\mathbf{v_e}(\omega)\\ \mathbf{v_{pc}}(\omega)\end{Bmatrix}=\begin{bmatrix}\mathbf{Y_s^{11}}(\omega) & -\mathbf{Y_s^{12}}(\omega)\\ \mathbf{0} & \mathbf{Y_c}(\omega)\end{bmatrix}\begin{Bmatrix}\mathbf{F_e}(\omega)\\ \mathbf{F_p}(\omega)\end{Bmatrix}, \tag{4}$$

which arises from rearranging Eq. (1). The expressions for the time-averaged transmitted power P^t are then synthesized in the frequency domain from the interfacial forces and velocities via

$$P^t(\omega)=\frac{\omega}{2\pi}\sum_k\int_0^{2\pi/\omega}\dot{\mathbf{q}}_k(t)\mathbf{F}_k(t)dt$$

$$=\frac{1}{2}\mathrm{Re}(\mathbf{v}^{\mathrm{H}}(\omega)\mathbf{F}(\omega))$$

where the superscript H denotes the Hermitian of a vector. Introduction of an inner product $\langle\mathbf{u},\mathbf{w}\rangle_{\mathbf{D}}=(\mathbf{Du})^{\mathrm{H}}\mathbf{w}$ and its corresponding norm $\|\mathbf{u}\|_{\mathbf{D}}^2=\langle\mathbf{u},\mathbf{u}\rangle_{\mathbf{D}}$ allows compact expression of these vibratory power flows.[13] Here $\mathbf{u}$ and $\mathbf{w}$ are arbitrary complex vectors, while $\mathbf{D}$ is any symmetric complex valued matrix. Due to the symmetry of $\mathbf{D}$, the norm possesses the properties $\mathrm{Re}(\|\mathbf{u}\|_{\mathbf{D}}^2)=\|\mathbf{u}\|_{\mathrm{Re}(\mathbf{D})}^2$ and $\mathrm{Im}(\|\mathbf{u}\|_{\mathbf{D}}^2)=\|\mathbf{u}\|_{\mathrm{Im}(\mathbf{D})}^2$, where Re( ) and Im( ) are the real and imaginary part operators, respectively. Using the inner product, the transmitted powers may be expressed as either quadratic forms of the excitation vector $\mathbf{F_e}$ or the free source velocity[9,10] by using the relationship $\mathbf{v_{sp}}(\omega)=\mathbf{Y_s^{21}}(\omega)\mathbf{F_e}(\omega)$. Since design modifications change the input power, $P_e^t(\omega)$, as well as the transmitted power, $P_{pc}^t(\omega)$, it is more convenient to present the ratio of the two as a comparison quantity. For instance, the power ratio for the transmission from the receiver to the foundation may be written as

$$\alpha_{pc}(\omega)=P_{\mathbf{pc}}^t(\omega)/P_e^t(\omega)$$

$$=\|\mathbf{F_e}(\omega)\|_{\mathbf{Q_{pc}}(\omega)}^2/\|\mathbf{F_e}(\omega)\|_{\mathbf{Q_e}(\omega)}^2 \tag{5a}$$

where the effective mobilities $\mathbf{Q}$ are

$$\mathbf{Q_e}(\omega)=\frac{1}{2}\mathrm{Re}(\mathbf{Y_s^{11}}(\omega)-\mathbf{Y_s^{12}}(\omega)\mathbf{\Gamma}(\omega)), \tag{5b}$$

$$\mathbf{Q_{pc}}(\omega)=\frac{1}{2}\mathrm{Re}((\mathbf{\Gamma}(\omega))^{\mathrm{H}}\mathbf{Y_c}(\omega)\mathbf{\Gamma}(\omega)), \tag{5c}$$

which describe how the excitation is filtered through the structure. Because the components are dissipative and the receiver, joint, and foundation are passive, the net power flow (i.e., summation of all paths at an interface) through the joint must be positive (out of the source) and the power ratios must always be less than unity. However the power flow through certain paths may actually be returned back into the source. The mobility method is particularly suited to the effort of reducing the power which is transmitted by the bearing paths. This is analogous to trying to achieve a high mobility (or impedance) mismatch.

One of the benefits of the mobility approach is the variety of methods by which the structural mobilities can be obtained. For instance, the appropriate elements of the equation

$$Y^{mn}(\omega)=i\omega[(\mathbf{K}-\omega^2\mathbf{M}+i\omega\mathbf{C})^{-1}]^{mn} \tag{6}$$

may be used, where the superscript mn refers to the element (m,n) of the matrix. It is this procedure which is used to quantify the compliant joint mobilities (with the mass matrix elements set to zero, since the joints are considered massless). The modal decomposition of this equation may also be utilized, which takes on the following form:

$$Y^{mn}(\omega)=i\omega\sum_r\frac{\phi_{r,m}\phi_{r,n}}{(\omega_r^2-\omega^2)+i\omega(2\zeta_r\omega_r)}, \tag{7}$$

where the modal properties can be obtained via analytical, experimental,[15,16] or finite element procedures. Note that Eq. (7) assumes proportional damping for the structure.

4. STUDY OF A GEARBOX

The simplified gearbox with rigid casing and gears, and compliant shafts and mountings is shown in Fig. 4. It exploits symmetry of the system to reduce the number of degrees of freedom. For the frequency range considered in this study, this model is reasonably valid.[7] The structure-borne sound can be transmitted to the casing and mounts via four bearings (each of which can transmit power via force/translations and moments/rotations) thereby necessitating a true vector approach. In this example, the dimension of the mobility matrices is 8 (since each bearing is assumed to possess only 2 degrees of freedom). This is a tractable problem.

A finite element program for this gearbox was created using beam elements for the shafts and generalized stiffness elements for the bearings and mounts. For the beam ele-

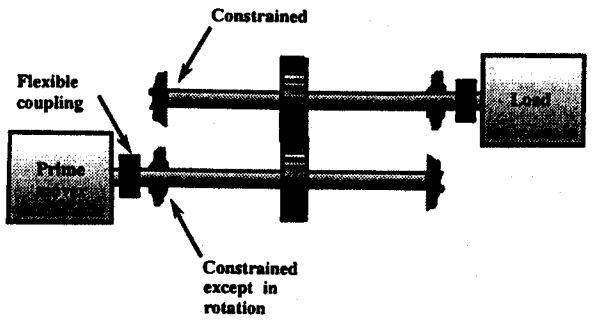

Fig. 4 – Schematic of the constrained source sub-system for the gearbox case.

ments, the stiffness (**K**) and consistent mass (**M**) matrices are

$$\mathbf{K}=\int_V (\partial\mathbf{N})\mathbf{D}(\partial\mathbf{N})^T dV, \tag{8a}$$

$$\mathbf{M}=\int_V \mathbf{N}\rho\mathbf{N}^T\, dV, \tag{8b}$$

where

$$\partial=\begin{bmatrix} \frac{\partial}{\partial z} & 0 \\ 0 & \frac{\partial}{\partial y} \\ \frac{\partial}{\partial y} & \frac{\partial}{\partial z} \end{bmatrix}=\begin{bmatrix} \frac{1}{l}\frac{\partial}{\partial \xi} & 0 \\ 0 & \frac{\partial}{\partial y} \\ \frac{\partial}{\partial y} & \frac{1}{l}\frac{\partial}{\partial z} \end{bmatrix}, \tag{8c}$$

$$\mathbf{N}=[\mathbf{N}_1 \quad \mathbf{N}_2], \tag{8d}$$

$$\mathbf{D}=\begin{bmatrix} E & \nu E & 0 \\ \nu E & E & 0 \\ 0 & 0 & G \end{bmatrix}, \tag{8e}$$

where E and ν are the modulus of elasticity and Poisson's ratio, respectively, and $\mathbf{N}_1$ and $\mathbf{N}_2$ are the finite element shape functions. The stiffness matrix has a flexural and a shear component as

$$\mathbf{K}=\frac{1}{l}\int_\xi\int_A \frac{\partial\mathbf{N}_1}{\partial\xi}E\frac{\partial\mathbf{N}_1^T}{\partial\xi}dA\, d\xi+\int_\xi\int_A\left(\frac{\partial\mathbf{N}_1}{\partial y}+\frac{1}{l}\frac{\partial\mathbf{N}_2}{\partial\xi}\right)G\left(\frac{\partial\mathbf{N}_1}{\partial y}+\frac{1}{l}\frac{\partial\mathbf{N}_2}{\partial\xi}\right)^T l\, dA\, d\xi. \tag{8f}$$

A variety of beam theories and elements have been developed to demonstrate the importance of proper modeling, and some of these approaches will be compared. Since the shafts in the gearbox are relatively thick, shear deformations may become significant. Therefore, it seemed that thick beam theories (such as Mindlin and Timoshenko[17]) may be better. These were compared against thin beam theory (Bernoulli–Euler) which neglects shear deformations. The shape functions for these different beam elements are given elsewhere.[14,17] The Mindlin beam is the easiest to formulate, while the Timoshenko is the most difficult. However the Mindlin beam is prone to shear locking unless reduced integration is used. This is done by using one Gauss point in the integration instead of 3. The Timoshenko beam element yields the exact solution for the deflection of a thick beam (even with one element),[17] while the other elements deviate significantly (particularly the Euler element) unless a large number of elements are used. The different elements will be compared in Sec. 5. As will be discussed later, the Timoshenko element will be chosen as the benchmark for this reason.

The source structure matrices are assembled from the shaft matrices with the gear mesh properties (stiffness, mass) at the appropriate nodal locations. These source matrices are then partitioned into boundary/interface (b) degrees of freedom and interior (i) degrees of freedom as

$$\mathbf{K}_s=\begin{bmatrix} \mathbf{K}_s^{bb} & \mathbf{K}_s^{bi} \\ (\mathbf{K}_s^{bi})^T & \mathbf{K}_s^{ii} \end{bmatrix}. \tag{9}$$

A coordinate transformation matrix is used to minimize modal truncation errors by improving the static completeness of the source basis.[14] The transformation is characterized by

$$\begin{Bmatrix} \mathbf{u}_s^b \\ \mathbf{u}_s^{i'} \end{Bmatrix}=\begin{bmatrix} \mathbf{I} & \mathbf{0} \\ \mathbf{A}_s^b & \mathbf{\Psi}_s^{cl} \end{bmatrix}\begin{Bmatrix} \mathbf{u}_s^b \\ \boldsymbol{\eta}_s^{j'} \end{Bmatrix}, \tag{10a}$$

$$\mathbf{\Gamma}_s=\begin{bmatrix} \mathbf{I} & \mathbf{0} \\ \mathbf{A}_s^b & \mathbf{\Psi}_s^{cl} \end{bmatrix}, \tag{10b}$$

where $\mathbf{A}_s^b=-(\mathbf{K}_s^{ii})^{-1}\mathbf{K}_s^{ib}$ and $\mathbf{\Psi}_s^{cl}$ represent the interior Lanczos vectors subject to constrained boundary conditions at the interfaces; see Fig. 4.

The generating algorithm for these Lanczos vectors[18] chooses the static displacement of the constrained interior problem as the first Lanczos vector. This ensures static completeness of the basis which minimizes truncation errors.[14] This is the reason the Timoshenko element was chosen for the shafts, since accurate representation of the static deflection is essential to the Lanczos procedure. The other beam elements will not yield the correct static deflection even in the absence of truncation.[16] A dynamic (Guyan) reduction algorithm was incorporated into this program[18] to further improve its computational efficiency.

Using the modal expansion of Eq. (7), the source mobility matrix becomes

$$\mathbf{Y}_s(\omega)=i\omega(\mathbf{L}_s\mathbf{\Phi}_s)(\mathbf{\Lambda}_s-\omega^2\mathbf{I}_s+i\omega\mathbf{\Xi}_s)^{-1}(\mathbf{L}_s\mathbf{\Phi}_s)^T, \tag{11a}$$

where the diagonal modal frequency, modal damping, and modal mass matrices are

$$\mathbf{\Lambda}_s=\mathbf{\Phi}_s^T(\mathbf{\Gamma}_s^T\mathbf{K}_s\mathbf{\Gamma}_s)\mathbf{\Phi}_s, \tag{11b}$$

$$\mathbf{\Xi}_s=\mathbf{\Phi}_s^T(\mathbf{\Gamma}_s^T\mathbf{C}_s\mathbf{\Gamma}_s)\mathbf{\Phi}_s, \tag{11c}$$

$$\mathbf{I}_s=\mathbf{\Phi}_s^T(\mathbf{\Gamma}_s^T\mathbf{M}_s\mathbf{\Gamma}_s)\mathbf{\Phi}_s \tag{11d}$$

and the modes are contained in $\mathbf{\Phi}_s$. Note that the dimension of these matrices ($\mathbf{\Phi}_s$, $\mathbf{\Lambda}_s$, $\mathbf{\Xi}_s$ and $\mathbf{I}_s$) may be significantly less than that of the original system matrices ($\mathbf{M}_s$, $\mathbf{C}_s$ and $\mathbf{K}_s$) because $\mathbf{\Gamma}_s$ is a rectangular matrix with as few Lanczos

vectors as possible. Most of the computational savings are achieved by these procedures therefore warranting the extra effort required in the formulation of $\mathbf{Y}_s(\omega)$. Also the Boolean selection matrix in (10a) is given by

$$\mathbf{u}_s^b = \mathbf{L}_s \begin{Bmatrix} \mathbf{u}_s^b \\ \eta_s^{1'} \end{Bmatrix} \tag{12}$$

which extracts the interface degrees of freedom from the displacement vector. The mobility matrix for the paths includes all of the bearings, such that

$$\mathbf{Y}_p(\omega) = i\omega \text{ diag } (\mathbf{K}_p^1 + i\omega\mathbf{C}_p^1, \mathbf{K}_p^2 + i\omega\mathbf{C}_p^2, \mathbf{K}_p^3 + i\omega\mathbf{C}_p^3, \mathbf{K}_p^4 + i\omega\mathbf{C}_p^4)^{-1}, \tag{13a}$$

where there are symmetric 2×2 stiffness and damping matrices for each of the four bearings

$$\mathbf{K}_p^\mu = \begin{bmatrix} K_p^{u_y u_y} & K_p^{u_y \theta_x} \\ K_p^{\theta_x u_y} & K_p^{\theta_x \theta_x} \end{bmatrix}, \tag{13b}$$

$$\mathbf{C}_p^\mu = \begin{bmatrix} C_p^{u_y u_y} & C_p^{u_y \theta_x} \\ C_p^{\theta_x u_y} & C_p^{\theta_x \theta_x} \end{bmatrix} \tag{13c}$$

for $\mu = 1\text{-}4$, which account for moment coupling, via $K_p^{u_y \theta_x}$ and $K_p^{\theta_x \theta_x}$. This is an important aspect of power transmission that is often neglected. In other studies, the bearings are usually only characterized by their radial stiffnesses, $K_p^{u_y u_y}$.

For the foundation, four mounts are considered with only axial stiffnesses and damping

$$\mathbf{K}_b = \text{diag } (K_b^1, K_b^2, K_b^3, K_b^4), \tag{14a}$$

$$\mathbf{C}_b = \text{diag } (C_b^1, C_b^2, C_b^3, C_b^4). \tag{14b}$$

The casing is assumed to have no flexibility. Thus it only possesses inertia properties

$$\mathbf{M}_a = \text{diag}(m_a^x, I_a^x, I_a^z). \tag{15}$$

The foundation mobility matrix is given by

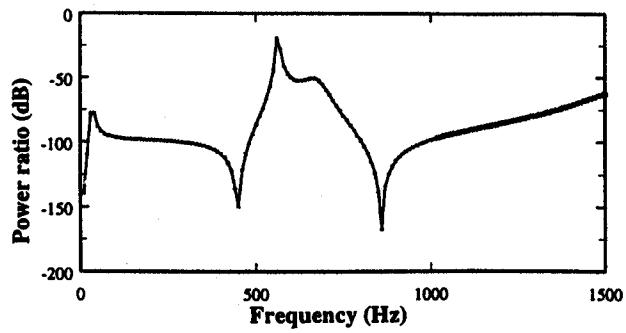

Fig. 5 – Validation of the proposed method for the gearbox via the structure-borne noise power ratio α_{pc}. — exact, ···· proposed method.

$$\mathbf{Y}_b(\omega) = i\omega \mathbf{P}_p^T (\mathbf{P}_b^T (\mathbf{K}_b + i\omega\mathbf{C}_b)\mathbf{P}_b - \omega^2 \mathbf{M}_a)^{-1} \mathbf{P}_p. \tag{16}$$

Furthermore, there are transformation matrices, one relates the displacements at the bearing locations to those of the rigid casing's center of gravity ($\mathbf{P}_p$), and another relates the displacements at the mount locations to those of the rigid casing's center of gravity ($\mathbf{P}_b$).

$$\mathbf{P}_p = \begin{bmatrix} 1 & 0 & 1 & 0 & 1 & 0 & 1 & 0 \\ -R_p^{z,1} & 1 & -R_p^{z,2} & 1 & -R_p^{z,3} & 1 & -R_p^{z,4} & 1 \\ R_p^{x,1} & 0 & R_p^{x,2} & 0 & R_p^{x,3} & 0 & R_p^{x,4} & 0 \end{bmatrix}, \tag{17a}$$

$$\mathbf{P}_b = \begin{bmatrix} 1 & -R_b^{z,1} & R_b^{x,1} \\ 1 & -R_b^{z,2} & R_b^{x,2} \\ 1 & -R_b^{z,3} & R_b^{x,3} \\ 1 & -R_b^{z,4} & R_b^{x,4} \end{bmatrix}, \tag{17b}$$

where $R_p^{x,i}$ and $R_p^{z,i}$ are the x and z components of the vector connecting the ith bearing to the casing center of gravity and $R_b^{x,j}$ and $R_b^{z,j}$ are the x and z components of the vector connecting the jth mount to the casing center of gravity.

For this system, the proposed method has been validated as shown in Fig. 5. The comparison of the power flow to the flexible mounts between the proposed synthesis and exact methods show excellent agreement. Here the exact method refers to the direct or unsynthesized approach. This is to be expected since the synthesis procedure is exact only when the complete modal basis of each structure is used. Nonetheless, a Guyan reduction technique was used on each structure to drastically reduce the dynamic degrees of freedom by a factor of about four. An excellent match was still achieved.

5. STUDY OF AN EXPERIMENTAL SETUP

The second model, shown in Fig. 2, is a further simplification of the gearbox. The structure is comprised of a 330×432×6.35 mm plate which represents the endplate of the gearbox, and a 127×229×6.35 mm plate intended to represent the meshing gears. Also two 12.7-mm-diam 381-mm-long shafts connect the two plates via bolted connections. Actual bearings were not used in this case since no method currently exists to experimentally obtain the mobility matrix of bearings. The joints were modeled as short beam elements which are intended to account for any compliance effects associated with the bolted connections. In the finite element model, beam elements are used for the shafts while shell elements are used for the plates. The gearshaft system is considered to be the source structure, and the casing is considered the receiver. The calculation of the interfacial forces proceeds as before, except that the intermediate matrices are now slightly different since the joints are beam elements

$$\mathbf{\Gamma}(\omega) = (\mathbf{Y}_c(\omega) + i\omega\mathbf{H}_p/(1 + i\omega\eta) + \mathbf{T}_p^T \mathbf{Y}_s^{22}(\omega)\mathbf{T}_p)^{-1} (\mathbf{Y}_s^{12}(\omega)\mathbf{T}_p)^T, \tag{18}$$

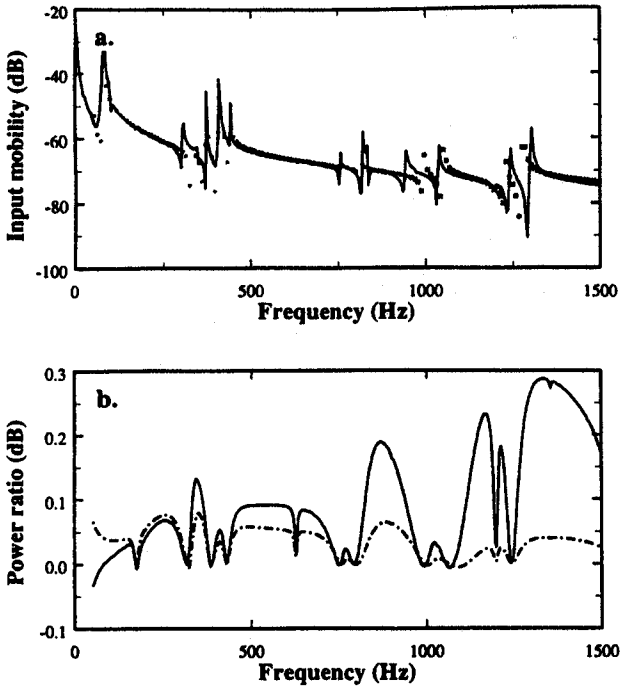

Fig. 6 – Validation of the proposed method for the experimental setup. (a) Input structural mobility, Y^e—experiment; ···· theory. (b) Transmitted power ratios, α_{pc}, for upper joint, —moment path; —·—·force path.

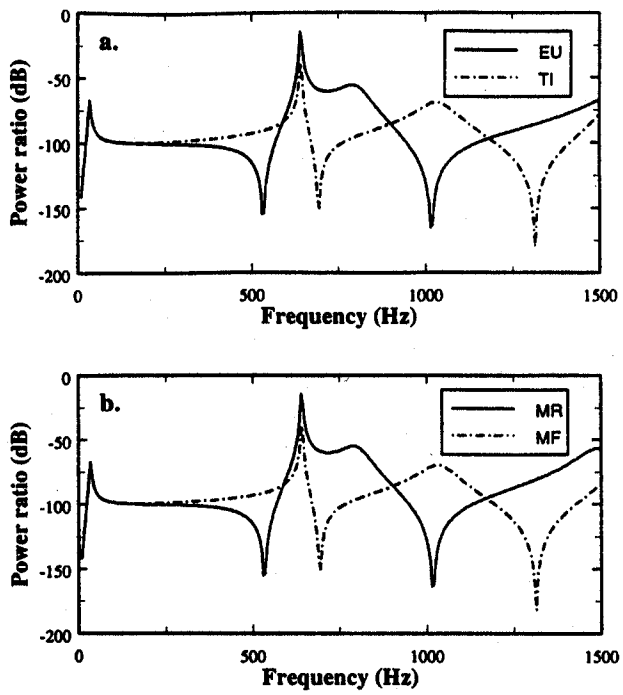

Fig. 7 – Comparison of different beam elements used to model gearbox shafts. Key: EU, Euler (B-spline) beam element; TI, Timoshenko beam element; MR, Mindlin beam element with reduced integraton; MF, Mindlin beam element with full integration.

where η is the joint loss factor and the matrix $\mathbf{T_p}$ represents the coupling between rotational and translational displacements

$$T_p^{\mu,\mu}=1.0, \quad \mu=1,\ldots,12, \tag{19a}$$

$$T_p^{2\nu,2\nu-1}=-l_\nu, \tag{19b}$$

$$T_p^{2\nu+2,2\nu+1}=l_\nu, \quad \nu=1,2. \tag{19c}$$

Furthermore the joint mobility is now related to the joint compliance

$$\mathbf{H_p}=\mathrm{diag}(\mathbf{H_p^1},\mathbf{H_p^2}), \tag{20}$$

where 1 and 2 refer to the upper and lower joint respectively. Each joint block may be further partitioned into the flexural compliances ($\mathbf{H_1^\nu}$ and $\mathbf{H_2^\nu}$) of each plane and the torsional/longitudinal compliances ($\mathbf{H_3^\nu}$)

$$\mathbf{H_p^\nu}=\mathrm{diag}(\mathbf{H_1^\nu},\mathbf{H_2^\nu},\mathbf{H_3^\nu}), \quad \nu=1,2, \tag{21a}$$

where

$$\mathbf{H_1^\nu}=\frac{l_\nu}{12E_\nu I_\nu}\begin{bmatrix}(4+\beta_\nu)l_\nu^2 & -6l_\nu\\ -6l_\nu & 12\end{bmatrix}, \tag{21b}$$

$$\mathbf{H_2^\nu}=\frac{l_\nu}{12E_\nu I_\nu}\begin{bmatrix}(4+\beta_\nu)l_\nu^2 & 6l_\nu\\ 6l_\nu & 12\end{bmatrix}, \tag{21c}$$

$$\mathbf{H_3^\nu}=\begin{bmatrix}l_\nu/E_\nu A_\nu & 0\\ 0 & l_\nu/G_\nu J_\nu\end{bmatrix}, \quad \nu=1,2, \tag{21d}$$

where β_ν is the shear deformation parameter associated with Timoshenko beam elements. The effective input mobility is also changed in this case to

$$\mathbf{Q_e}(\omega)=\frac{1}{2}\mathrm{Re}(\mathbf{Y_s^{11}}(\omega)-(\mathbf{T_p^T Y_s^{21}}(\omega))^T\mathbf{\Gamma}(\omega)). \tag{22}$$

The transmitted power ratios are calculated as before.

6. TYPICAL RESULTS

The model for the experimental setup yields encouraging results, as evident from Fig. 6(a) which compares theoretical and experimental input mobilities. This quantity is directly related to the power input into the structure by Eq. (1a). Though not shown here, other quantities such as the free source velocity also yielded good matches. This model permits the study of how the flexural motions in the shafts, as induced by the gear mesh forces, transmit noise to the casing. Since the out-of-plane motion response of the plate is primarily due to the moment coupling of the bearings, the power flow properties of the joints or bearings become very important. Figure 6(b) confirms the dominance of the moment path, especially at higher frequencies. Also observe the role of system resonances.

As discussed earlier, the shafts may be modeled with a variety of elements. A comparison of the results using different beam elements in the gearbox model is given in Fig. 7. The Timoshenko element will be considered the benchmark since it is exact for thick beams. The Euler element predicts the natural frequencies incorrectly, as does the

Mindlin element with reduced integration which produces nearly identical results. The Mindlin element with full integration however yields results similar to the Timoshenko, and although it is certainly the easiest to formulate, it is not selected since it may be prone to shear locking. Therefore, from Fig. 7 and the earlier discussion about static completeness, the importance of choosing the proper elements in the model is confirmed.

To show the importance of a proper model for the bearings, results for different bearing stiffness properties are compared in Fig. 8. The usual modeling of only radial stiffness, or only diagonal terms, yields significant discrepancies in the power flows. This confirms the importance of including the translational-rotational transfer stiffness.

7. SOME VIBRO-ACOUSTIC DESIGN CRITERIA

From the mobility equations developed here for the power flow to the foundation one can readily observe some important vibro-acoustic design principles: (1) keep receiving structure (i.e., gearbox) mobility as low as possible (2) maintain joint (i.e., bearing) mobility as high as possible, and (3) increase source structure (i.e., gears and shafts) mobility as much as possible. However, in a geared system the misalignments and excessive deflections which would result from overly compliant shafts and bearings are obviously undesirable. Thus only the first design criterion, making the gearbox as rigid as possible, seems viable for such systems. However the other two criteria may be realized to a lesser degree by increasing the source and joint damping, which has also been suggested by other authors[1,19,20] based on different approaches. This is illustrated in Fig. 9(a) where the bearing/joint damping was increased. At the lower frequencies this modification has minimal effect, but it becomes increasingly important at the higher frequencies. The reason that not much improvement was realized is because there is little relative motion across the bearings in the frequency range considered. Thus, little power is dissipated in the bearings before being transmitted to the casing. This becomes an important design trade-off as dissipation must be increased while misalignment is reduced. Further, if the bearings are softened or stiffened as shown in Fig. 9(b) the effect is noticeable at the higher frequencies.

Other studies of the simplified gearbox concentrate on how eccentricities introduced through asymmetry affect the structural power flow. Here the comparison quantities will be the total transmitted power ratios through the bearings broken up into force and moment paths. Originally, the center of gravity is assumed to coincide with the gear mesh, and the mounts are symmetrically distributed about the mesh line of action as shown in Fig. 10. For instance, if the rigid casing's center of gravity is shifted along the z axis, the power transmitted by the force path through the bearings is unaffected [Fig. 11(a)], while that transmitted via the moment path is somewhat altered. However, if the center of gravity is shifted along the x axis, a noticeable change occurs in the power flow through both paths (Fig. 12). In particular, the moment power flow is significantly increased. When the gear mesh is shifted such that there are unequal lengths of shaft on either side (while maintaining

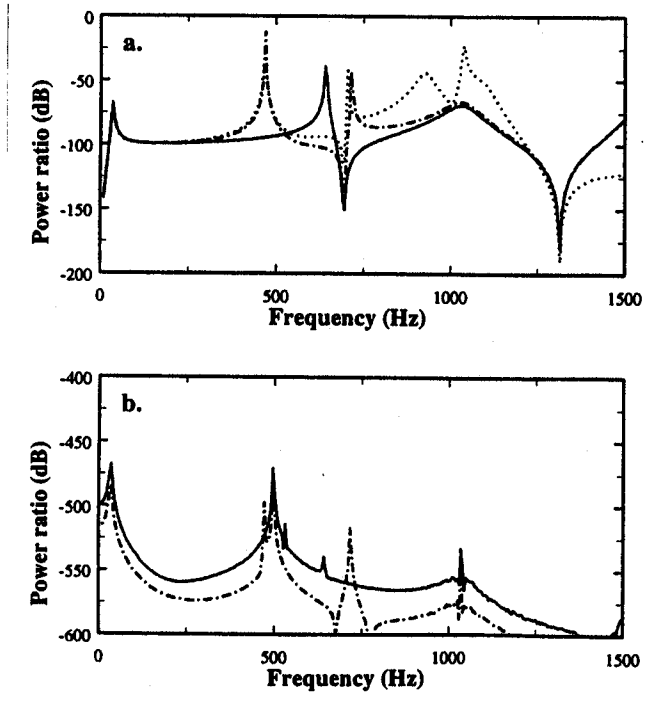

Fig. 8 – Comparison of different bearing stiffnesses for the gearbox. (a) Force path. (b) Moment path. Key: —original stiffness [Fig. 7(a)]; —·—·diagonal stiffness (no coupling term); ····only radial stiffness.

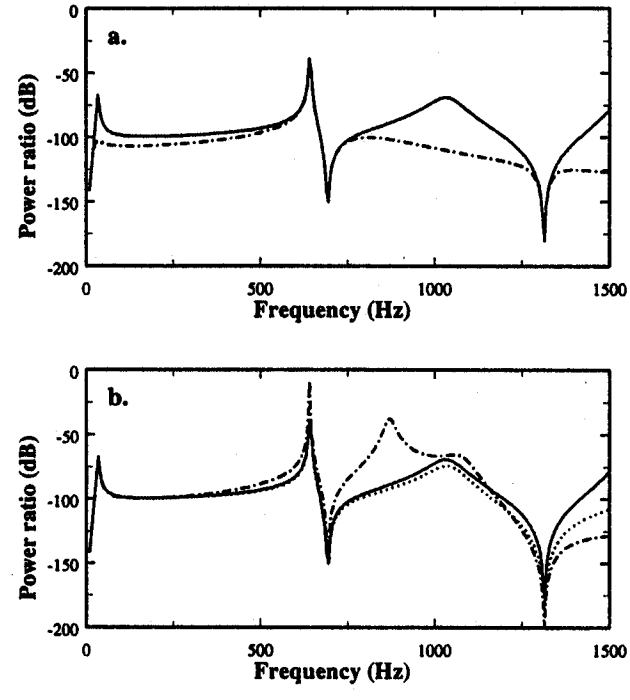

Fig. 9 – Effects of bearing properties on structure-borne noise power ratio, α_{pc}, for a gearbox. (a) effect of bearing damping: —original damping [Fig. 7(a)]; —·— increased damping. (b) effect of bearing stiffness: —original stiffness [Fig. 7(a)]; —·—·decreased stiffness; ····increased stiffness.

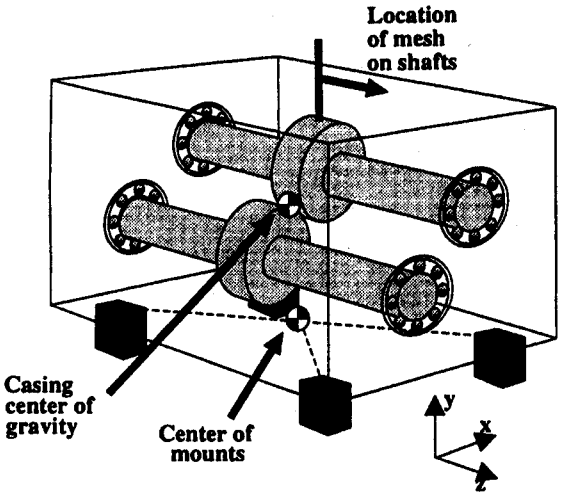

Fig. 10 – Schematic of gearbox parameters.

the same total lengths of shafts), there again seems to be little change in the force path [Fig. 13(a)], and a more noticeable effect in the moment path. The location of the mounts also affects the power flows. When the distribution of the mounts is asymmetric with respect to the z axis, only the moment path shows some difference [Fig. 14(b)]. However, when the mounts are asymmetric with respect to the x axis the moment power flows are significantly amplified [Fig. 15(b)]. These results suggest that the power flows are more sensitive to asymmetries along the x axis (transverse

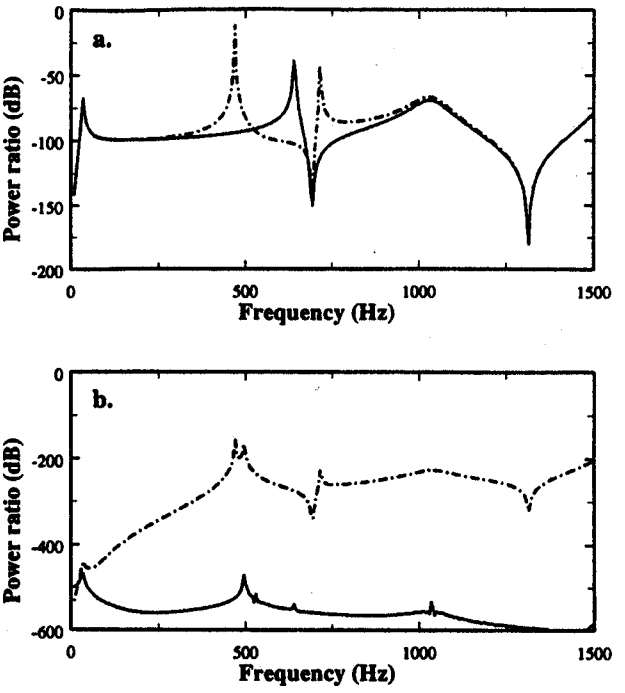

Fig. 12 – Effect of increasing eccentricity in x direction between casing center of gravity and mesh location by shifting casing center of gravity. (a) α_{pc}, force path, (b) α_{pc}, moment path. Key: —original; —·—·shifted.

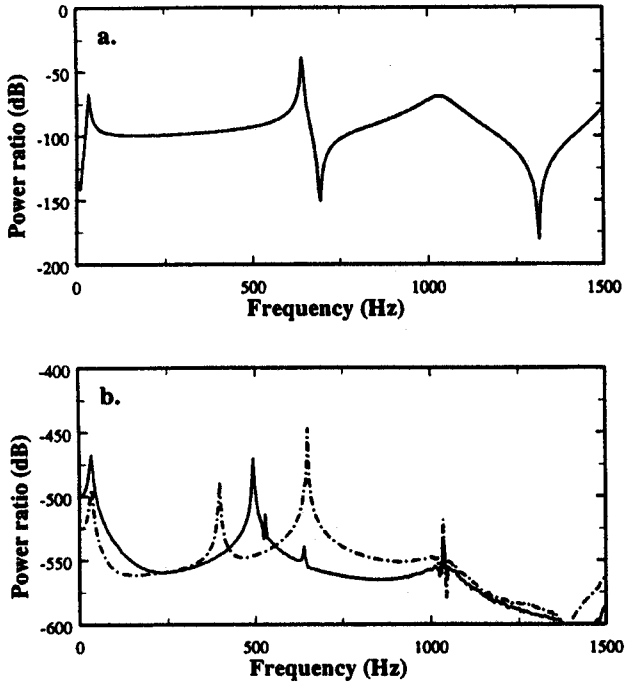

Fig. 11 – Effect of increasing eccentricity in z direction (along gearbox shafts) between casing center of gravity and mesh location by shifting casing center of gravity. (a) force path. (b) α_{pc}, moment path. Key: —original; —·—·shifted.

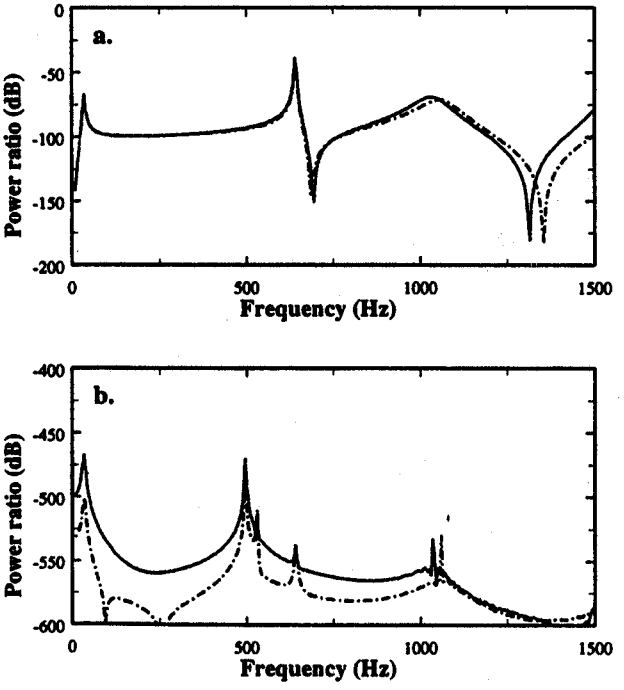

Fig. 13 – Effect of increasing eccentricity between casing center of gravity and mesh location by increasing asymmetry in shafting length. (a) α_{pc}, force path. (b) α_{pc}, moment path. Key: —original; —·—·shifted.

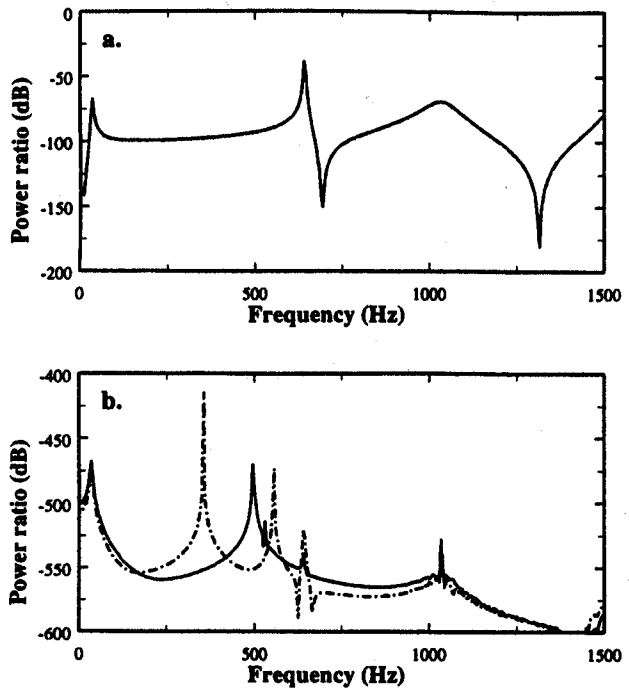

Fig. 14 – Effect of increasing eccentricity in z direction (along shafts) between geometric center of mounts and mesh location. (a) α_{pc}, force path, (b) α_{pc}, moment path. Key: — original; —·—· shifted.

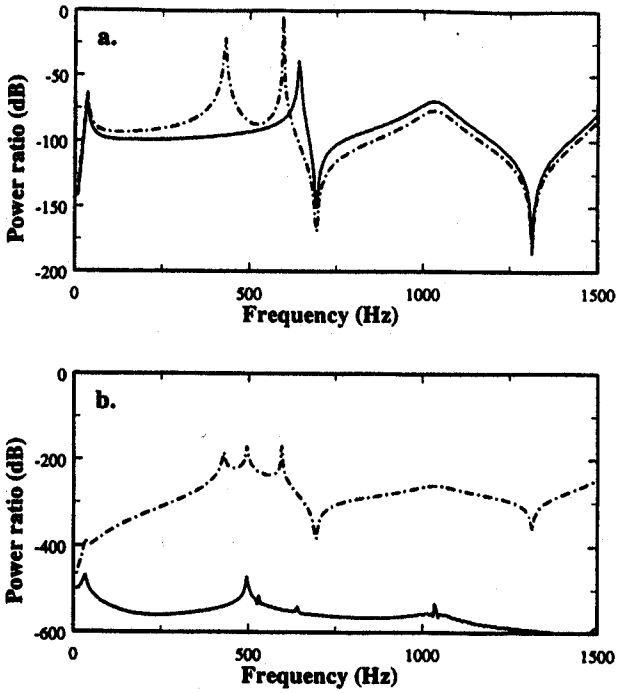

Fig. 15 – Effect of increasing eccentricity in x direction between geometric center of mounts and mesh location. (a) α_{pc}, force path. (b) α_{pc}, moment path. Key: — original; —·—· shifted.

to the shafts). This is because the eccentricities along this axis add equally to all of the bearing positions, while shifting along the z axis increases the distance to (i.e., moment arm) two bearings while decreasing the distance to the other two.

8. CONCLUSION

This study supports the validity and applicability of the proposed analytical method as well as the importance of the bearings to the structure-borne power flow. The proposed method is capable of handling non-ideal joints and vector path information and is an improvement upon prior analysis methods. Due to the reduced dimension of the method, it is well suited for computer-aided design implementation, as well as efficient vibro-acoustic parametric design studies. Also the modeling of the gearbox, as well as the algorithm, has been specifically chosen so that truncation errors are avoided. The effects of the bearing properties and asymmetries in the system have been investigated through conceptual studies. Even though simplified gearbox-like structures have been considered here, the methodology presented could be applied to more realistic models of mechanical drives. In future research, casing compliance needs to be examined further from the noise viewpoint. Also, a method to experimentally determine the *in-situ* noise performance of the bearings is desirable.

ACKNOWLEDGMENTS

This study was supported by the U.S. Army Research Office [URI Grant DAAL 03-92-G0120; 1992-97; Project Monitor: Dr. T.L. Doligalski]. A previous version of this paper was presented by Todd E. Rook as part of the student paper contest at NOISE-CON 94.

REFERENCES

[1] P. K. Brandl, "Design Strategies for Low Noise Engine Concepts," SAE Paper 911070 (1991).
[2] D. B. Welbourn, "Fundamental Knowledge of Gear Noise-A Survey," IMechE Trans. 9–14 (1979).
[3] H. Opitz, "Noise of Gears," Philos. Trans. R. Soc. London **263**, 369–380 (1968).
[4] A. N. S. Van Roosmalen, "Design Tools for Low Noise Gear Transmissions," Ph.D. thesis, Eindhoven Univ. of Tech. (1994).
[5] R. J. Drago, J. W. Lenski, Jr., and A. Royal, "An Analytical Approach to the Source Reduction of Noise and Vibration in Highly Loaded Mechanical Power-Transmission Systems," Proc. 5th World Cong. on Theory of Mach. and Mech. 910–913 (1979).
[6] R. Singh, Gear Noise Short Course Notes, The Ohio State University (1993).
[7] T. C. Lim and R. Singh, "Vibration Transmission Through Rolling Element Bearings, Part I," J. Sound Vib. **139**(2), 179–199 (1990).
[8] J. Cuschieri, "Vibration Transmission through Periodic Structures using a Mobility Power Flow Approach," J. Sound Vib. **143**(1), 65–74 (1990).
[9] J. M. Mondot and B. Petersson, "Characterization of Structure-borne Sound Sources: the Source Descriptor and the Coupling Function," J. Sound Vib. **114**(3), 507–518 (1987).
[10] B. Petersson and J. Plunt, "On Effective Mobilities in the Prediction of Structure-borne Sound Transmission Between a Source Structure and a

Receiving Structure, Part I: Theoretical Background and Basic Experimental Studies," J. Sound Vib. **82**(4), 517–529 (1982).
[11] J. Farstad, M. R. Lee, and R. Singh, "Analysis of Structure-borne and Radiated Sound using Component Modal Bases," Appl. Acoust. **43**, 217–246 (1994) .
[12] J. Farstad and R. Singh, "Effects of Modal Truncation Errors on Transmitted Dynamic Power Estimates in Discretely Joined Component Assemblies," J. Acoust. Soc. Am., in press (1996).
[13] T. E. Rook and R. Singh, "Power Flow Through Multi-Dimensional Compliant Joints Using Mobility and Modal Approaches," J. Acoust. Soc. Am. **97**(5), 1–10 (1995).
[14] T. E. Rook and R. Singh, "Modal Truncation Issues in Synthesis Procedures for Vibratory Power Flow and Dissipation," J. Acoust. Soc. Am., in press (1996).
[15] D. D. Kana and L.M. Vargas, "Prediction of Payload Vibration Environments by Mechanical Admittance Test Techniques," NASA Cont. Rpt. 2591 (1975).
[16] D. D. Kana and L. M. Vargas, "Transient Excitation and Mechanical Admittance Test Techniques for Prediction of Payload Vibration Environments," NASA Cont. Rpt. 2787 (1977).
[17] S. S. Lee, J. S. Koo, and J. M. Choi, "Variational Formulation for Timoshenko Beam Element by Separation of Deformation Mode," Comm. Num. Methods Eng. **10**, 599–610 (1994).
[18] J. S. Przemieniecki, *Theory of Matrix Structural Analysis* (McGraw-Hill, New York, 1968).
[19] P. Schwibinger, D. Hendrick, W. Wu, and Y. Imanishi, "Noise and Vibration Control Measures in the Powertrain of Passenger Cars," SAE Paper 911053 (1991).
[20] J. Woodhouse, "An Approach to the Theoretical Background of Statistical Energy Analysis Applied to Structural Vibration," J. Acoust. Soc. Am. **69**, 1695–1709 (1981).